DRFC/CAD

EUR-CEA-FC-1623

Heat Flux Driven Ion Turbulence

X. Garbet, R.E. Waltz

Janvier 1998

CEA EURATOM

ASSOCIATION EURATOM-C.E.A.
DEPARTEMENT DE RECHERCHES
SUR LA FUSION CONTROLEE
CEA/CADARACHE
13108 SAINT PAUL LEZ DURANCE CEDEX

Heat Flux Driven Ion Turbulence

X. Garbet
Association Euratom-CEA sur la Fusion, Bat. 513,
CEA/Cadarache,13108 St Paul lez Durance, France
R.E. Waltz
General Atomics, P.O. Box 85608,
San Diego, California 92186-9784

Abstract

This work is an analysis of an ion turbulence in a tokamak in the case where the thermal flux is fixed and the temperature profile is allowed to fluctuate. The system exhibits some features of Self-Organized Critical systems. In particular, avalanches are observed. Also the frequency spectrum of the thermal flux exhibits a structure similar to the one of a sand pile automaton, including a 1/f behavior. However, the time average temperature profile is found to be supercritical, i.e. the temperature gradient stays above the critical value. Moreover, the heat diffusivity is lower for a turbulence calculated at fixed flux than at fixed temperature gradient, with the same time averaged temperature. This behavior is attributed to a stabilising effect of avalanches.

I. INTRODUCTION

Heat transport in tokamaks is known to exhibit unexpected features. The question of scaling laws and fast transients is of particular interest. In the traditional picture of turbulence in tokamak plasma turbulence, the correlation lengths L_c scale as an ion Larmor radius ρ_{s0}, and correlation times τ_c scale as a minor radius divided by the acoustic speed a/c_{s0}. A simple random walk estimate yields the so called gyroBohm scaling $\chi_{Ti} \equiv \chi_{gB} = \rho_{s0}^2 c_{s0}/a$. Furthermore, the same argument implies that the typical propagation time of a heat pulse should be of the order of a^2/χ_{Ti}, which also gives a rough estimate of the confinement time. These elementary predictions appear to disagree with recent experimental results. It has been shown that the confinement scaling law

does not always follow the gyroBohm prediction in L mode[1-2]. Fast transients have been observed to take place within time scales two order of magnitude smaller than a confinement time[3-4]. Several explanations have been proposed to explain these discrepancies. The first is based on the fact that the radial width of linear eigenmodes (the so called global modes) scale as $\sqrt{a\rho_{s0}}$ [5-6]. Using this linear scaling in a random walk estimate leads to a Bohm scaling. A second explanation relies on the stabilizing effect of a rotational shear flow (diamagnetic phase velocity plus diamagnetically induced ExB drift). This effect results in a correlation length scaling as ρ_{s0}, but decorrelation rates which decrease when increasing ρ_{s0}. The stabilization process leads to gyroBohm scaling far above critical temperature profiles but worse than Bohm scaling near threshold [7].

Our paper is motivated by a third explanation emphasizing the apparently non local plasma response, which was recently proposed by Diamond and Hahm[8]. This approach is related to the concept of Self-Organized Criticality (SOC)[9,10], for which the paradigm is a sand pile (more precisely a cellular automaton simulating a sand pile). In SOC models, avalanches play a central role[9,10]. In a tokamak plasma, an avalanche corresponds to a fast radial propagation of a heat pulse. The mechanism can be understood as follows. A heating burst induces locally a transient steepening of the temperature profile. Once the temperature gradient exceeds the turbulence threshold, this steepening induces a burst of turbulence which expels the heat outward. The process is then renewed at the neighbouring radial position. A necessary condition for such a behavior is the existence of a turbulence threshold and a conservation law (here energy conservation). In sand pile numerical models, avalanches occur at all spatial and time scales. One consequence is a 1/f behavior of the frequency spectrum, which is commonly observed in these simulations[10]. Also, it is generally found that the time average slope of a sand pile is sub-critical, i.e. it stays below the threshold value, at least for small source rates (most of the sand piles can always get "laminar" flow at sufficently high source rates). For a class of models, this behavior corresponds to a diffusive equation for

which the diffusion coefficient is singular[11]. As emphasized by Diamond and Hahm, avalanches induce correlations lengths of the temperature profile which scale as the minor radius, and not as an ion Larmor radius, thus breaking the gyroBohm prediction. Furthermore, the propagation may be ballistic and the time scale is much shorter than a diffusive time scale. The key question here is to know whether such a model can be applied to a tokamak turbulence. It is important to realize that the avalanche effect cannot be seen in a system where the long length scale temperature gradient is fixed. This is actually the case in most of numerical simulations of tokamak turbulence. Carreras et al. proposed a numerical realisation of a SOC based on a resistive interchange instability in a cylinder[12]. Some of their results can be summarized as follows:

- the time Fourier spectrum of the turbulent energy at a given position exhibits a 1/f behavior

- fast propagation of pulses is observed: the behavior is diffusive for an outward propagation. An inward propagation is ballistic.

- the time average temperature profile is sub-critical, i.e., the gradient is below the critical value.

These results are similar to those for a sand pile model used for a tokamak plasma[13]. Similar results have been obtained for a turbulence driven by a particle flux in the Scrape-Off Layer (SOL) of a tokamak. This question was studied with an automaton representing the coupled dynamics of particles and neutrals[14] and with a fluid code computing a 2D interchange turbulence in the SOL[15]. In both cases, avalanches were shown to play an important role. Some indications of self-organization were also found in particle simulations of an ion turbulence[16] . However, the existence of avalanches is not mentioned in the latter work.

The purpose of the present work is to investigate an ion turbulence with a simplified two dimensional (2D) full radius code that was used to study scaling laws with shear flow[7]. This code has been modified to operate at fixed heat flux, and no scale separation is performed for the heat equation. The code is simplified in the sense that the radial shape of each Fourier harmonic with

respect to poloidal and toroidal directions is given and fixed. This allows a fast computation while keeping the main features of toroidal ITG turbulence. Parallel field line ion dynamics driving "slab-like" ITG modes is not included. We find that avalanches occur, resulting in the characteristic 1/f behavior of the flux and turbulent energy Fourier spectra. This behavior confirms that fast transport transients across the discharge are possible. However, the system is always super-critical, i.e. the gradient of the time average temperature profile stays above the threshold. When the dissipation in the heat equation is very small, the system remains close to marginal stability whatever the heat flux, but is not found to be sub-critical everywhere. For more relevant levels of dissipation in tokamaks, the system can be driven away from marginality when increasing the power source. An important result is that the turbulent heat diffusivity is larger when the temperature profile is fixed than when it is allowed to fluctuate. This result is attributed to the stabilizing effect of avalanches.

The remainder of the paper is as follows. Section II deals with the formulation of the 2D model. Results concerning the dynamics of the temperature profile are given in section III. Section IV deals with heat transport and scaling laws. A conclusion follows in section V.

II. A MODEL FOR ION TURBULENCE

A. Fluid equations

We use a cylindrical equilibrium with the coordinates (r,θ,φ). Density, pressure and electric potential are written under the form:

$$[n_i, p_i, \phi](r,\theta,\varphi,t) = [n_{eq}, p_{eq}, \phi_{eq}](r) + \sum_{m,n} [n_i, p_i, \phi]_{m,n}(r,t)\exp\{i(m\theta + n\varphi)\} \qquad (1)$$

We start here with a set of fluid equations proposed by Nordman and Weiland[17] for toroidal ITG modes

$$\begin{aligned} &\partial_t n_i + \mathbf{v}_{\perp i}.\nabla n_i = -n_i \nabla.\mathbf{v}_{\perp i} \\ &\partial_t p_i + \mathbf{v}_{\perp i}.\nabla p_i = -5/3 p_i \nabla.\mathbf{v}_{\perp i} - 2/3 \nabla.\mathbf{q}_{\perp i} + S \end{aligned} \qquad (2)$$

where

$$\mathbf{v}_{\perp i} = \mathbf{v}_E + \mathbf{v}^*_{pi} + \mathbf{v}_{pol}$$

$\mathbf{v}_E$is the electric drift velocity, $\mathbf{v}^*_{pi}$ is the diamagnetic velocity, $\mathbf{v}_{pol}$ accounts for the polarisation drift and Finite Larmor Radius (FLR) effects, $\mathbf{q}_{\perp i}$ is the perpendicular heat flux and S(r) is the heat source. More precisely

$$\begin{aligned}
\mathbf{v}_E &= \frac{\mathbf{B}\times\nabla\phi}{B^2} \\
\mathbf{v}^*_{pi} &= \frac{\mathbf{B}\times\nabla p_i}{n_i e_i B^2} \\
\nabla.(n_i \mathbf{v}_{pol}) &= -\nabla.\left\{\frac{n_i m_i}{e_i B^2}\left(\partial_t + \left(\mathbf{v}_E + \mathbf{v}^*_{pi}\right).\nabla\right)\phi\right\} \\
\mathbf{q}_{\perp i} &= \frac{5}{2} p_i \mathbf{v}^*_{Ti} \quad \mathbf{v}^*_{Ti} = \frac{\mathbf{B}\times\nabla T_i}{e_i B^2}
\end{aligned} \tag{3}$$

The parallel motion is ignored here. Introducing the derivative $d_t = \partial_t + \mathbf{v}_E.\nabla$, the system can be recast under the form

$$\begin{aligned}
d_t n_i - \nabla.\left\{\frac{n_i m_i}{e_i B^2}\left(\partial_t + \left(\mathbf{v}_E + \mathbf{v}^*_{pi}\right).\nabla\right)\phi\right\} &= n_i\left(\mathbf{v}_E + \mathbf{v}^*_{pi}\right).\frac{2\nabla B}{B} \\
d_t p_i &= \frac{5}{3} p_i\left(\mathbf{v}_E + \mathbf{v}^*_{pi} + \mathbf{v}^*_{Ti}\right).\frac{2\nabla B}{B}
\end{aligned} \tag{4}$$

where a low β assumption has been made to calculate the curvature term. We introduce here the following normalisations

$$\begin{aligned}
r \to \bar{r} = \frac{r}{\rho_{s0}} \quad t \to \bar{t} = \frac{c_{s0} t}{a} \quad \nabla \to \bar{\nabla} = \rho_{s0}\nabla \\
n_i \to N_i = \frac{a}{\rho_{s0}}\frac{n_i}{n_0} \quad \phi \to \Phi = \frac{a}{\rho_{s0}}\frac{e_i\phi}{T_{e0}} \quad p_i \to P = \frac{a}{\rho_{s0}}\frac{p_i}{p_{e0}}
\end{aligned} \tag{5}$$

where n_{e0}, T_{e0}, p_{e0} are reference values (these are not the values on the magnetic axis), $c_{s0} = \sqrt{T_{e0}/m_i}$ is the acoustic speed, $\rho_{s0} = m_i c_{s0}/e_i B_0$ is the corresponding ion Larmor radius, and « a » is the minor radius. The ion temperature profile is supposed to be proportional to the electron temperature profile, τ being the ratio T_i/T_e. We assume scale separation for the ion density density allowing n_i to commute with the gradient in Eq (4a). We define the normalised profile $\hat{n}(r,t)$ as

$$\hat{n}(r,t) = \int_0^{2\pi} \frac{d\theta d\varphi}{4\pi^2} n_i(r,\theta,\varphi,t)/n_{e0} \tag{6}$$

In practice, the normalised density profile $\hat{n}(r,t)$ is fixed (it does not depend on time) and flat so that these simplications are not very important. Definitions similar to Eq. (6) hold for the normalised profiles $\hat{T}(r,t), \hat{p}(r,t)$. The system (4) then becomes

$$\begin{aligned} &d_{\bar{t}} N_i - \hat{n}\bar{\nabla}.\left\{d_{\bar{t}}\nabla\Phi\right\} - \tau\hat{n}\bar{\nabla}.\left\{v_{pi}^*.\nabla\Phi\right\} = \omega_D.(\hat{n}\Phi + \tau P) \\ &d_{\bar{t}} P = \frac{5}{3}\omega_D.\left(\hat{p}\Phi - \hat{T}^2\tau\bar{n}_i + 2\tau\hat{T}P\right) \end{aligned} \tag{7}$$

where

$$\omega_D = -i\frac{2a}{R}\left(\cos(\theta)\partial_{\bar{r}} + \sin(\theta)\frac{1}{\bar{r}}\partial_\theta\right) \tag{8}$$

and

$$d_{\bar{t}} = \partial_{\bar{t}} + \left[\partial_{\bar{r}}\Phi\frac{1}{\bar{r}}\partial_\theta - \frac{1}{\bar{r}}\partial_\theta\Phi\partial_{\bar{r}}\right] \tag{9}$$

where we approximate n_i/n_{e0} by $\hat{n}$ and p_i/p_{e0} by $\hat{p}$ in the curvature terms. We make further aproximations. For simplicity the diamagnetic part of the non linear advection term is entirely neglected in Eq.(7a) so that linear finite Larmor radius (FLR) terms are dropped. The consequence is a rather inaccurate threshold. This is not crucial, since the exact computation of diffusivities is not the purpose here. For helical modes, the relevant quantity is therefore the combination $N_i - \hat{n}\bar{\nabla}_\perp^2\Phi$. The electron density fluctuations are linked to the potential fluctuations through the Boltzmann relation

$$n_e(r,\theta,\varphi,t) - n_{eq}(r) = \frac{\hat{n}(r,t)}{\hat{T}(r,t)}\left(\phi(r,\theta,\varphi,t) - \phi_{eq}(r)\right) \tag{10}$$

Using quasineutrality n_e=n_i, we introduce a generalized vorticity

$$N = \hat{n}\left(\lambda\frac{\Phi}{\hat{T}} - \nabla_\perp^2\Phi\right) = f^{-1}.\Phi \tag{11}$$

where λ=0 for m=0,n=0 radial modes and λ=1 for helical m,n fluctuations, the system (7) becomes

$$\begin{aligned} &d_{\bar{t}} N = -i\omega_n^*.f.N + i\omega_D.(\hat{n}f.N + \tau P) \\ &d_{\bar{t}} P = \frac{5}{3}i\omega_D.\left(\hat{p}f.N - \hat{T}^2\tau N + 2\tau\hat{T}P\right) + S \end{aligned} \tag{12}$$

The linearised version of the system (12) for the poloidal (m) and toroidal (n) components is

$$\begin{aligned}\partial_{\bar{t}} N_{mn} &= -i\omega_n^*.f.N_{mn} + i\left[\omega_D.(\hat{n}f.N + \tau P)\right]_{mn} \\ \partial_{\bar{t}} P_{mn} &= -i\omega_p^*.f.N_{mn} + \frac{5}{3}i\left[\omega_D.\left(\hat{p}f.N - \hat{T}^2\tau N + 2\tau\hat{T}P\right)\right]_{mn}\end{aligned} \tag{13}$$

where

$$\left(\omega_n^*.N\right)_{mn} = -a\frac{dn_{eq}}{n_{eq}dr}\frac{im}{r}\rho_{s0}N_{mn} \tag{14}$$

This operator vanishes for radial modes.

B. Quasi-ballooning representation

The equations above do not account for the parallel dynamics. The latter effects are known to localise the m,n Fourier components in the radial direction around the corresponding resonant surface $r = r_{mn}$ such that $q(r_{mn}) = -m/n$, where q is the safety factor. To introduce this effect, each m,n mode is developed over a given set of orthonormal functions W_ℓ

$$[N,P]_{m,n}(\bar{r},\bar{t}) = \sum_\ell [N,P]_{m,n,\ell}(\bar{t})W_\ell\left(\frac{r - r_{mn}}{\Delta_{m,n}}\right) \tag{15}$$

Here, the set is limited to two functions, even (ℓ=0) and odd (ℓ=1). This is the minimum required to keep a non-vanishing geodesic curvature and account for shear flow generation. There functions are chosen to be gaussians, whose width $\Delta_{m,n}$ is proportional to the local ion Larmor radius

$$\rho_s(r_{mn},t) = \rho_{s0}\left[\hat{T}(r_{mn},t)\right]^{1/2}.$$

In the same way, the radial profiles are developed over a set of basis functions W_k

$$\begin{aligned}[N,P]_{eq}(r,t) &= \sum_k [N,P]_k(t)W_k(r) \\ W_k(r) &= \frac{J_0\left(\pi\alpha_k\frac{r}{a}\right)}{J_1(\pi\alpha_k)}\end{aligned} \tag{16}$$

where J_0, J_1 are Bessel functions and α_k is the k-th zero of $J_0(\pi r/a)$. The set $\{W_k\}$ is orthonormal[18]. Note that this procedure imposes that all fields

vanish at r=a. The system (12) is then projected onto these m,n and radial shape functions. This reduces the dimensionality to two. More details have been given in previous work[7,19].

C. Sources and dissipation

A dissipation has to be added in Eqs(12) to account for collisional and Landau damping. For m,n Fourier modes, this dissipation has been chosen as

$$d_{\bar{t}} = \partial_{\bar{t}} + v_E.\nabla_{\bar{r}} - \mu_0 - \mu_1\left(\rho_s \frac{m}{r}\right)^2 - \mu_2\left(\rho_s \frac{m}{r}\right)^4 \qquad (17)$$

where $[\mu_0, \mu_1, \mu_2]$ are adjustable parameters. For radial modes, a diffusion operator

$$d_{\bar{t}} = \partial_{\bar{t}} + v_E.\nabla_{\bar{r}} - \bar{\mu}\frac{1}{\bar{r}}\partial_{\bar{r}}\bar{r}\partial_{\bar{r}} \qquad (18)$$

is used, where $\bar{\mu}$ is an ion neoclassical heat diffusivity. While this choice is suitable for the pressure, it is not suitable for the generalized vorticity radial modes, since a pure diffusion operator would provide a vanishing radial electric field without turbulent flow generation. This contradicts the fact that the radial electric field is finite in a tokamak without toroidal rotation. Neglecting the neoclassical diamagnetic poloidal rotation, the electric field compensates the ion pressure gradient. This means that the overall poloidal velocity of ions cancels. To account for this effect, the vorticity equation is written as

$$\begin{aligned} &\partial_{\bar{t}} N_{eq} + \frac{1}{\bar{r}}\partial_{\bar{r}}\bar{r}\Gamma_N = -\bar{\mu}\left(N_{eq} - \frac{1}{\bar{r}}\partial_{\bar{r}}\bar{r}\partial_{\bar{r}}P_{eq}\right) \\ &\Gamma_N = \sum_{m,n} i\frac{m}{\bar{r}} N_{mn}\Phi^*_{mn} \end{aligned} \qquad (19)$$

where the second term represents the turbulent flow generation and $N_{eq} = -(\hat{n}/\bar{r})\partial_{\bar{r}}\bar{r}\partial_{\bar{r}}\Phi$ (see Eq.(11)). In the case where the flow generation contribution vanishes, and for a flat density profile, Eq.(19), with the above boundary conditions, guarantees that the time average of the radial electric field is the opposite of the time average pressure gradient. In other words, the ExB velocity is balanced against the diamagnetic velocity and ions do not flow.

Since the temperature profile is allowed to fluctuate, it has to be sustained by a heat source. This source term is of the form

$$S(r) = S_0 \hat{S}(r)$$

$$\hat{S}(r) = \frac{\bar{S}(r)}{\frac{1}{a^2}\int_0^a \bar{S}(r) r dr} \quad ; \bar{S}(r) = \exp\left\{-4\frac{r_S^2}{r^2} - \frac{r^2}{w_S^2}\right\} \tag{20}$$

This source term exhibits a maximum at $r = \sqrt{2 r_S w_S}$, and is such that it decreases rapidly when approaching the axis. The reason for this choice is the lack of resonant magnetic surfaces close to the axis, which implies that the turbulence vanishes in this region. This can lead to non physical large pressure gradients when the diffusion $\bar{\mu}$ is small, except if the thermal flux is also small. The form given by Eq.(20) insures that the thermal flux is small close to the magnetic axis. The equation for the pressure radial modes is therefore

$$\begin{aligned} &\partial_{\bar{t}} P_{eq} + \frac{2}{3}\frac{1}{\bar{r}}\partial_{\bar{r}} \bar{r} \Gamma_T = \bar{\mu}\frac{1}{\bar{r}}\partial_{\bar{r}} \bar{r} \partial_{\bar{r}} P_{eq} + S \\ &\Gamma_T = \frac{3}{2}\sum_{m,n} i\frac{m}{\bar{r}} P_{mn} \Phi_{mn}^* \end{aligned} \tag{21}$$

where Γ_T is the heat flux. This gives the instantaneous turbulent heat diffusivity

$$\chi_{Ti} = \chi_{gB} \frac{\Gamma_T}{-\hat{n} a \frac{d\hat{T}}{dr}} \tag{22}$$

where $\chi_{gB} = \rho_{s0}^2 c_{s0} / a$ is the gyroBohm reference value. It will be useful to define the time average heat diffusivity, with time average values of Γ_T and $d\hat{T}/dr$. The link between the source amplitude and the total input power P_{input} is given by the relation

$$P_{input} = 3 n_0 T_0 V \frac{\rho_{s0} c_{s0}}{a^2} S_0 \tag{23}$$

where $V = 2\pi R \pi a^2$ is the volume. In this model, the edge gradient adjusts itself such the time average of the heat outflux balances the input flux, which is the radial integral of the source S.

D. Numerical simulations

The initial temperature profile is

$$\hat{T}(r) = \left(1 - r^2/a^2\right)^2 \tag{24}$$

whereas the fixed density profile is given by

$$\hat{n}(r) = \left[0.9\left(1 - r^2/a^2\right)^2 + 0.1\right]^{1/10} \tag{25}$$

and is flat in the core. The radial profile of the safety factor is chosen to be linear $q(r) = q_{min} + (q_{max} - q_{min})(r/a)$, where $q_{min} = 0.95$ and $q_{max} = 3.05$. The toroidal wavenumber n ranges between n_{min} and n_{max} with a step Δn. For each toroidal wavenumber n, a poloidal wavenumber m is kept only if the mode m,n is resonant (i.e. there exists a magnetic surface such that $q(r_{mn}) = -m/n$). In what follows, $\rho_{s0}/a = 0.01$, $n_{min} = 10$, $n_{max} = 100$ and $\Delta n = 10$, unless other values are specified. This corresponds to 796 odd and even m,n modes. The number of radial modes is 20. The width of the m,n radial shape functions $W_\ell\left((r - r_{mn})/\Delta_{m,n}\right)$ is chosen such as $\Delta_{m,n} = 7.5 q(r_{mn}) \rho_s(r_{mn})/q_{max}$. The time scheme is an explicit predictor-corrector with a time step of $1.25\ 10^{-2}\, a/c_{s0}$. The dissipation for m,n modes is determined by μ_0=0.05, μ_1=0, and μ_2=0.7 whereas for radial modes $\bar{\mu} = 0.1$. The role of the latter parameter will be discussed. The source parameters are r_s=0.2a, and w_s=0.15a, such that the maximum of the source pofile is close to r=0.25a. The interesting region for confinement is thus located between 0.2 and 1 in normalised radius. For such a flat density profile, the threshold is essentially characterised by a critical temperature gradient length. For an aspect ratio R/a=3 and τ=1, this threshold is given by $a dT_i/T_i dr$=-1.8. If the temperature gradient is kept fixed, the code is fast since the non linear coupling coefficients are computed at the beginning of the run and stored. However if the temperature $\hat{T}$ in the system (12) as well as the local ion Larmor radius are time dependent functions, the coupling coefficients have to be recalculated. Updating these coupling coefficients every $25\, a/c_{s0}$ is sufficient. This means in practice that only the temperature gradient is a fast fluctuating quantity and not the temperature $\hat{T}$ which evolves slowly.

III. TEMPERATURE PROFILE

A. Instantaneous and time average profiles

Fig.1 shows an example of instantaneous and time average profiles of temperature for a source amplitude S_0=0.01. This case will be refered in the following as the reference case. Clearly, the temperature profile at a given time exhibits a radial sequence of flat and steep regions. These plateaux are transient, as indicated by the time average profile, which is smooth. As will be shown in the next section, the life time of a plateau is a few times a / c_{s0}, i.e. a few μs in a real tokamak. Such a plateau is the result of a transient quasilinear flattening.

B Avalanches

An interesting question deals with the dynamics of these oscillations of the temperature profile. A heating induces locally a steepening of the gradient, which exceeds the turbulence threshold and thus produces an increase of the turbulent heat flux, expelling the flux toward a larger radius. At this new position, this burst of heat will again increase the temperature and increase the turbulence. This process can be repeated many times, such as a domino effect. This process is known as an « avalanche » in SOC systems[9]. Fig.2 shows contour plots of the heat flux and pressure as functions of radial position and time. They clearly show large scale events, that can be assimilated to avalanches. These contour plots show that there exists partial avalanches, that occur over a finite radial extent, and large scale events, that propagate all over the plasma size. Large scale events are also apparent on the time evolution of the thermal flux at a given radial position, as shown on Fig.3. There are no evident characteristic spatial and time scales for partial avalanches. Following the works of Hwa and Kardar[10], and Carreras et al.[12], this can be diagnosed by computing the Fourier transform of the thermal flux and the turbulent energy,

as indicated on Fig.4. These spectra exhibit a characteristic shape which consists of three parts:

- a low frequency part, which behaves as ω^0. Following the interpretation of Hwa and Kardar, this corresponds to large scale events.

- an intermediate range, which behaves as $\omega^{-0.9}$, which corresponds to partial avalanches. This behavior is close to the $1/\omega$ behavior that is observed in sand pile models[9]. It is indicative of the lack of characteristic scale for the avalanches.

- a high frequency part, which behaves as $\omega^{-2.3}$, and corresponds to isolated events. The exponent is close to the one observed in sand piles models (-2).

C. Stability

To this point, the system exhibits some features of a SOC system, and these results are close to those obtained by Carreras et al.[12] for a resistive interchange turbulence. Here, we address the issue of profile stability. It was indeed found by Carreras et al. that the pressure profile is sub-critical, i.e. stays on average below the critical value. We investigate this question by calculating the growth rates at a given instant of time, and also the rates deduced from the time average of the temperature profile. One can actually define two kinds of linear growth rates: the local growth rates, which correspond to the ballooning representation at the lowest order, and the global growth rates (the exact values), which correspond to global eigenmodes. The local growth rate is obtained in the following manner. Considering a peculiar resonant magnetic surface m_0, n, it is assumed that the gradients are constant and equal to their actual values on this surface. An exact linear solution is of the form

$$[N_{mn\ell}, P_{mn\ell}] = [N_{n\ell}, P_{n\ell}] \exp\{i(m - m_0)\theta_0\} \qquad (26)$$

where θ_0 is the ballooning angle and the odd and even components (labelled by ℓ) are coupled. After a scan over the ballooning angle, this procedure provides a set of frequencies $\omega_{loc}(m,n)$, associated to the resonant surfaces $r = r_{mn}$. A

local growth rate $\gamma_{loc}(r)$ is then computed by taking in each interval [r,r+dr] the maximum value among the growth rates $\mathrm{Im}\{\omega(m,n)\}$ such that the corresponding resonant surface $r_{m,n}$ lays within this interval. The global growth rates are deduced from the eigenvalues of the linear matrix (Eqs 13). An example of profile $\gamma_{loc}(r)$ is given on Fig.5. Two conclusions can be drawn:

- the local mode growth rate at a given time exhibits a radial sequence of negative (stable) and positive (unstable) regions. This obviously corresponds to the regions where the temperature is flat or steep.

- the local mode growth rate deduced from the time average temperature is positive everywhere. The system is therefore super-critical.

Positive values of the maximum global growth rates are found with both the instantaneous and time average temperature profiles. This conclusion is reinforced by looking at the profiles after a scan of the additional power (Fig.6). The expectation for a SOC system is a profile located below the marginal profile for source rates not exceedingly large. Starting from the standard case S_0=0.01 and dropping the source by a factor 10 leads to a profile close to marginality (growth rates do not exceed 0.01). This procedure thus determines the critical profile. Increasing the source from the standard case by a factor 2.5 drives the profile significantly away from the marginal profile. This is still more obvious for an increase by a factor 5. Thus, this system is super-critical. Nevertheless, and not surprisingly, it exhibits some resilience, i.e. the increase of temperature with additional power is not linear. Additional information is provided by the probability distribution function (pdf) of the ion temperature gradient length $adT_i/T_i dr$. The pdf at mid-radius is shown on Fig.7 for the standard case S_0=0.01. The mean value of the gradient length is -2.1 and is thus above the critical value -1.8. This shift increases towards the edge. The shape of this pdf is not far from a Gaussian (dashed line). However, an excess of events at large gradients is usually observed. The latter behavior is likely due to avalanches.

D. Role of the source and dissipation

This behavior is different from the one observed by Carreras et al[12]. There are at least two differences between these simulations: in the present case the dissipation for radial modes is larger and there is no external source of noise.

Dissipation plays an important role: a decrease of the dissipation increases the SOC character. More precisely, decreasing $\bar{\mu}$ down to 10^{-4} (i.e. a value much lower than the neoclassical prediction), it is found that the system is still super-critical but stays very close to the threshold, whatever the heating. Also, the plateaux are more pronounced. Interestingly, depletions of pressure are also observed to propagate upwards, as mentioned in previous works (see Fig.8) [8,12,19]. The explanation for the dependence of avalanches on dissipation is the following one: a plateau of width w is eroded by the background diffusion after a diffusion time $\tau_\mu = w^2 / \bar{\mu}$. The stabilising effect of a plateau will be fully efficient if this time is larger than a growth time $1/\gamma$. Since the latter time is of order 10 in a/c_{s0} units, this condition is only marginally satisfied for small plateaux whose width is of order of ρ_{s0} when $\bar{\mu} = 0.1$.

An external source of noise is different from the intrinsic noise induced by the turbulence, as emphasized in[20]. Many authors have studied this problem with a white noise assumption

$$\langle S(r,t)S(r+\rho,t+\tau)\rangle = 2D\delta(\rho)\delta(t) \qquad (27)$$

A noisy source approaching this condition in time has been implemented (it is described in the appendix). Numerical simulations indicate that adding such a source in the reference case does not change the above conclusion: the profile stays supercritical. However, using a less localised source plus a noise provides a system which is locally subcritical in the core r/a<0.4. An example with S_0=0.01, w_S=5a and S_{noise}=0.01 is shown in Fig.10. The fact that the turbulence level is substantial in a sub-critical region does not prove that this case is a realisation of a SOC system. It has been already shown that for an artificially weak dissipation, a turbulence can propagate from unstable to stable regions,

leading to a finite diffusivity in regions where the growth rates are locally negative[7,19].

IV. HEAT TRANSPORT

A Heat diffusivity

The presence of locally flat or inverted regions means the instaneous the heat diffusivity can be infinite or even negative in these plateau regions. However, here we refer to the time average heat diffusivity as defined earlier. An example is given on Fig.11. Note that the diffusivity does not decrease radially except in the extreme edge where the temperature, and therefore the mode widths, vanish. Also, the wiggling on the profile is indicative of persistent flattening of the temperature profile, corresponding to the most unstable modes.

B. Temperature gradient and heat flux driven turbulences

A critical question then arises: is the heat diffusivity calculated at fixed flux the same as the one computed with a turbulence driven by a fixed temperature profile? To answer this question, the turbulence is calculated with a fixed temperature profile given by the time average of the temperature in a heat flux driven turbulence. As described in the Appendix of Ref.[7], the local long scale temperature gradients are kept fixed to the time average value, by introducing "compensating" sources with non-smooth radial profiles. Also, the profile of equilibrium electric potential is frozen. As a consequence, the corresponding rotational shear flow stabilisation is the same (in average) in both simulations. Fig.11 shows that the diffusivity can be somewhat larger at fixed gradient than at fixed heat flux, for the same temperature profile. In this example the ratio of diffusivities is 1.3 in the core increasing to 2 at the edge. This is a general result, which indicates that avalanches play a global stabilizing role. This effect should be accounted for, when comparing local and global simulations.

V. CONCLUSION

This work shows that a simplified model for an ITG turbulence exhibits some features of SOC systems. In particular, the Fourier spectrum of the turbulent flux exhibits a 1/f behavior. This behavior can be attributed to avalanche like dynamics. However, in contrast with results from most of cellular automatons and a previous fluid model for plasma turbulence, the temperature profile is super-critical, i.e., the gradient stays above the threshold value. This departure from marginality increases with the heating flux. It has to be stressed here that the diffusivity for more physical simulations at fixed heat flux is somewhat less than for fixed temperature, even if the time average of the temperature profile is the same. We attribute this to the time average stabilizing effect due to the occurrence of avalanches. Existence of avalanches provides a way to understand fast transients in transport which are sometimes observed in tokamaks. The question of scaling laws is still open and will be addressed in a future publication.

ACKNOWLEDGEMENTS

We want to thank Dr B. Carreras and Pr P. Diamond for pointing out the roles of external noise and dissipation in self-organisation. Fruitful discussions with Drs Y. Sarazin and P. Ghendrih have been appreciated.

APPENDIX: Implementation of a noisy source

A noisy source has been added in the heat equation as follows

$$\tilde{S}(r,\bar{t}) = S_{noise}\,U(\bar{t})V(r)$$

where

$$U(\bar{t}) = \sqrt{\frac{2}{N_t}}\sum_{\nu=1}^{N_t}\cos\left(2\pi\nu\frac{t}{T}+\varphi_\nu\right)$$

$$V(r) = \frac{\hat{V}(r)}{\int_0^a \frac{dr}{a}\frac{r}{a}\hat{V}(r)};\ \hat{V}(r) = \sum_{k=1}^{N_r}\frac{1}{1+0.2\left(\frac{\alpha_k}{\alpha_1}\right)^4}W_k(r) \qquad \text{(A1)}$$

and T is the average time, φ_ν are random phases between 0 and 2π. Defining an average

$$\left\langle F(r,\bar{t})\right\rangle_{r,\bar{t}} = \int_0^a 2\frac{dr}{a}\frac{r}{a}\int_0^T\frac{d\bar{t}}{T}F(r,\bar{t}) \qquad \text{(A2)}$$

one can easily check that $\left\langle S(r,\bar{t})\right\rangle_{r,\bar{t}} = 0$. The time auto-correlation is

$$C_U(\tau) = \left\langle U(t)U(t+\tau)\right\rangle_t = \frac{1}{N_t}\cos\left(\pi(N_r+1)\frac{\tau}{T}\right)\frac{\sin\left(\pi N_r\frac{\tau}{T}\right)}{\sin\left(\pi\frac{\tau}{T}\right)} \qquad \text{(A3)}$$

Up to a $1/N_t$ factor, the function C_U approaches a delta function in the limit of large N_t. It is of prime importance to check that the effect of this source is correctly computed. To achieve this goal, cases with a very low level of turbulence are computed. This is equivalent to solve a heat diffusion equation with a noisy source. In this particular case, the pdf of the pressure gradient should be gaussian at each radial position, with a standard deviation $\sigma(r)$ given by the relation

$$\sigma^2(r) = \left\langle\left(\frac{a\nabla p}{p_0}(r) - \left\langle\frac{a\nabla p}{p_0}(r)\right\rangle_{\bar{t}}\right)^2\right\rangle_{\bar{t}} = \qquad \text{(A4)}$$

$$\frac{S_{noise}^2 T}{2N_t\bar{\mu}}\sum_{k,k'=1}^{N_r} V_k V_{k'}\frac{1}{\pi^2\left(\alpha_k^2+\alpha_{k'}^2\right)}\frac{dW_k(r)}{dr}\frac{dW_{k'}(r)}{dr}$$

The space average of the variance σ^2 is

$$\left\langle \sigma^2(r) \right\rangle_r = \frac{S_{noise}^2 T}{2N_t \bar{\mu}} \left(\sum_k^{N_r} V_k \right)^2 \qquad \text{(A5)}$$

This behavior has been verified for the parameters T=8000, $\bar{\mu} = 10$ and $N_t = 250$. The pdf of pressure gradients are indeed found to be gaussian and the computed variance agrees with expression (A4). It has also been verified that there are no avalanches in this case. This test gives some confidence in the way the noise is computed.

For the turbulence case, we have chosen T=1000 and $N_t = 600$ in order to get a correlation time smaller than a / c_{s0}.

FIGURE CAPTIONS

Fig.1: Instantaneous and time average temperature profiles. The source amplitude is S_0=0.01, ρ^*=0.01 and the diffusion coefficient is $\overline{\mu} = 0.1$. Other parameters are given in section II.D.

Fig.2: Contour plots of thermal flux (a) and pressure (b) as function of the radial position and time. Same parameters as in Fig.1.

Fig.3:Time evolution of the thermal flux at mid-radius. Same parameters as in Fig.1.

Fig.4:Time Fourier transform of the thermal flux at mid-radius.

Fig.5:Radial profile of the local growth rate at a given time (solid line) and calculated with the time average temperature profile (dashed line). Same parameters as in Fig.1.

Fig.6:Time average temperature profiles for increasing values of the source amplitude.

Fig.7:Probability distribution function of the normalised temperature gradient. The dashed line is a gaussian fit and the continuous line is a fit over 8 Hermite functions.

Fig.8: Contour plots of thermal flux (a) and pressure (b) as function of the radial position and time. The source amplitude is S_0=0.01 and the diffusion coefficient is $\overline{\mu} = 10^{-4}$.

Fig.9: a) Pdf of pressure gradients at mid-radius for a run without turbulence with a noisy source as defined in the appendix. b) Comparison between the

computed standard deviation (solid line) and the theoretical expression (A4) (dashed line).

Fig.10: Profile for the local growth rate for the reference (solid line), for a case with a flatter source profile and an external noise (S_0=0.01, w_S = 5a and S_{noise}=0.01, dashed line). All growth rates are calculated with time averaged profiles.

Fig.11: Profile of diffusivities at fixed flux and at fixed temperature profile, where the latter is computed from the run at fixed flux. Same parameters as in Fig.1.

REFERENCES

[1] J.P. Christiansen, B. Balet, D. Boucher, C.D. Challis, J.G. Cordey, C. Gormezzano, C. Gowers, G. Kramer, D.G. Muir, S.V. Neudatchin, J. O'Rourke, G. Shmidt, P.M. Stubberfield, A. Taroni, F. Tibone, B. Tubbing, Plasma Phys. Controlled Fusion **34** , 1881 (1992).

[2] C.C. Petty, T.C. Luce, R.I. Pinsker, K.H. Burrell, S.C. Chiu, P. Gohil, R.A. James, D. Wroblewski, Phys. Rev. Lett. **74**, 1763 (1995).

[3] K. W. Gentle, W. L. Rowan, R. V. Bravenec, G. Cima, T. P. Crowley, H. Gasquet, G. A. Hallock, J. Heard, A. Ouroua, P. E. Phillips, D. W. Ross, P. M. Schoch, C. Watts, Phys. Rev. Lett. **74**, 3620 (1995).

[4] J.D. Callen, et al., to appear in Plasma Physics and Controlled Fusion (Proc. 24th Eur. Conf. Berchtesgaden, 1997)

[5] J. W. Connor, J. B. Taylor, and H. R. Wilson, Phys. Rev. Lett. **70**, 1803 (1993).

[6] F. Romanelli and F. Zonca, Phys. Fluids B **5**, 4081 (1993).

[7] X. Garbet and R. Waltz, Phys. Plasmas **5**, 1907 (1996)

[8] P.H. Diamond, T.S. Hahm, Phys. Plasmas **2**, 3640 (1995)

[9] P. Bak, C. Tang, and K. Wiesenfield, Phys. Rev. Lett. **59**, 381 (1987).

[10] T. Hwa and M.Kardar, Phys. Rev. A **45**, 7002 (1992).

[11] J.M. Carlson, J.T. Chayes, E.R. Grannan, and G.H. Swindle, Phys. Rev. Lett., **65**, 2547 (1990).

[12] B.A. Carreras, D. Newman, V.E. Lynch, and P.H. Diamond, Phys. Plasmas **3**, 2903 (1996)

[13] D.E. Newman, B.A. Carreras, P.H. Diamond, and T.S. Hahm, Phys. Plasmas **3**, 1858 (1996).

[14] Y. Sarazin, and Ph. Ghendrih, J. Nucl. Mat. **241-243**, 322 (1997).

[15] Y. Sarazin, Ph. Ghendrih, and X. Garbet, "Intermittent transport due to particle flux drive of SOL turbulence", to appear in Controlled Fusion and Plasma Physics (Proc. 24th EPS conference, Berchtesgaden,1997).

[16] Y. Kishimoto, T. Tajima, W. Horton, M.J. Lebrun, J.Y. Kim, Phys. Plasmas **3**, 1289 (1996)

[17] H. Nordman , J. Weiland, Nucl. Fusion **29**, 253 (1989).

[18] P.M. Morse, and H. Feshbach, in *Methods of Theoretical Physics*, (McGraw Hill, 1953), vol. II, p. 1260.

[19] L.P. Kadanoff, S. R. Nagel, L. Wu, and S. Zhou Phys. Rev. A **39**, 6524 (1989)

[20] J. A. Krommes, Physics Reports **283**, 5 (1997).

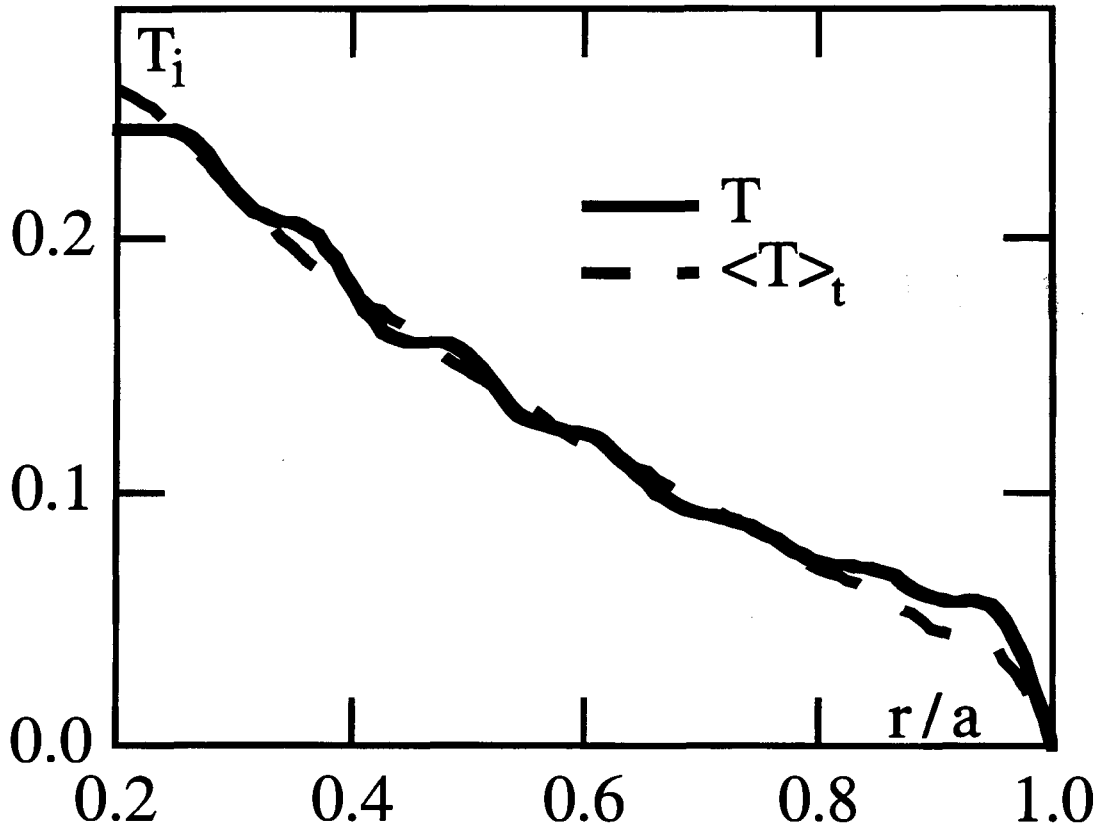

Fig.1

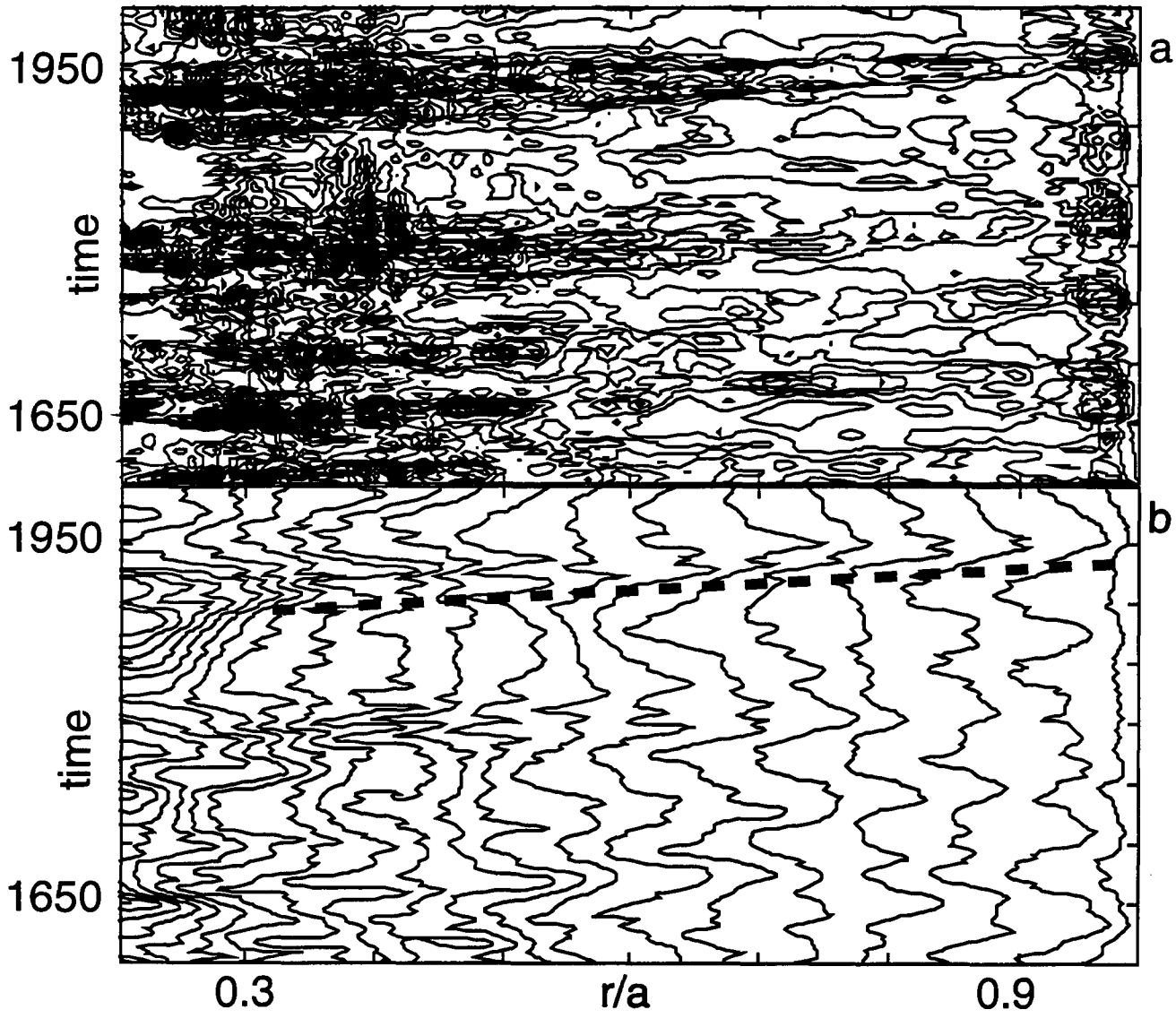

Fig.2

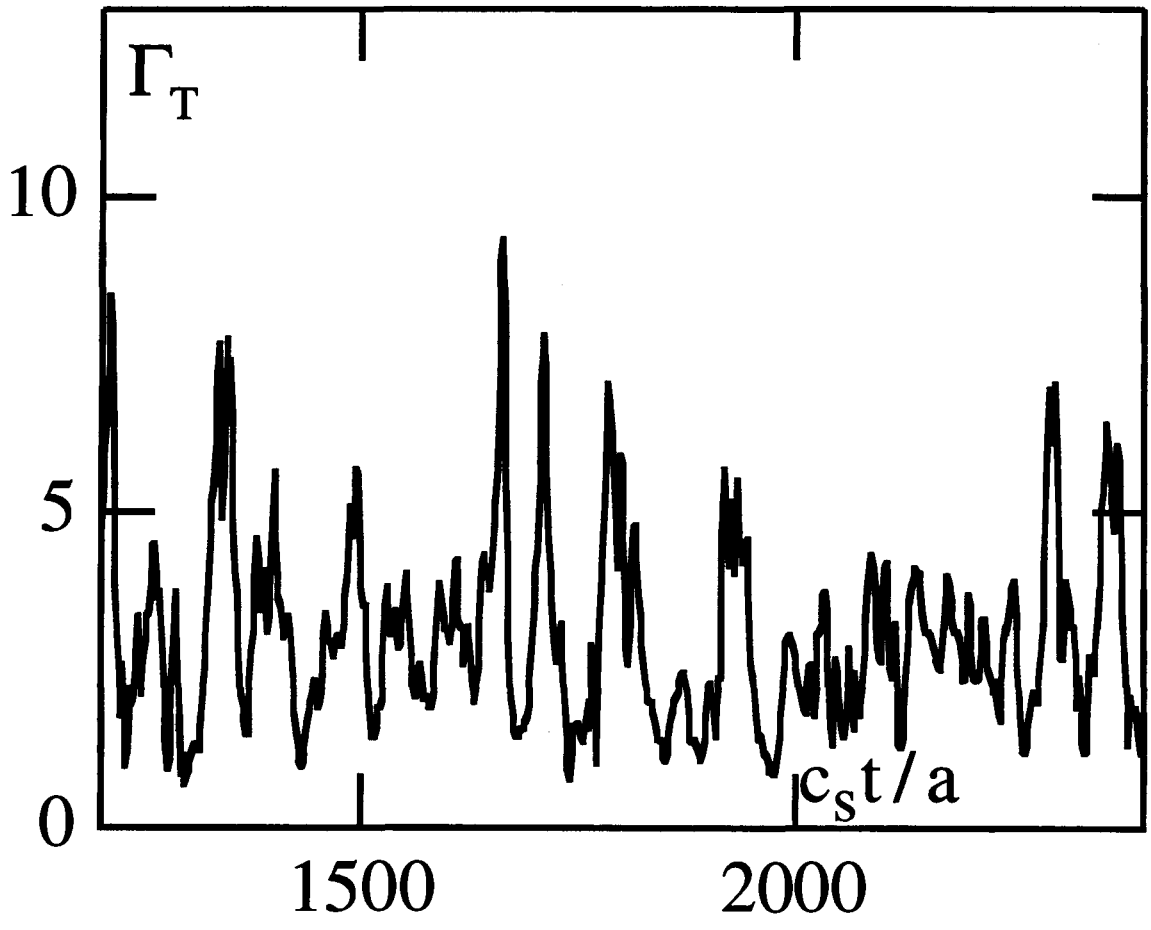

Fig.3

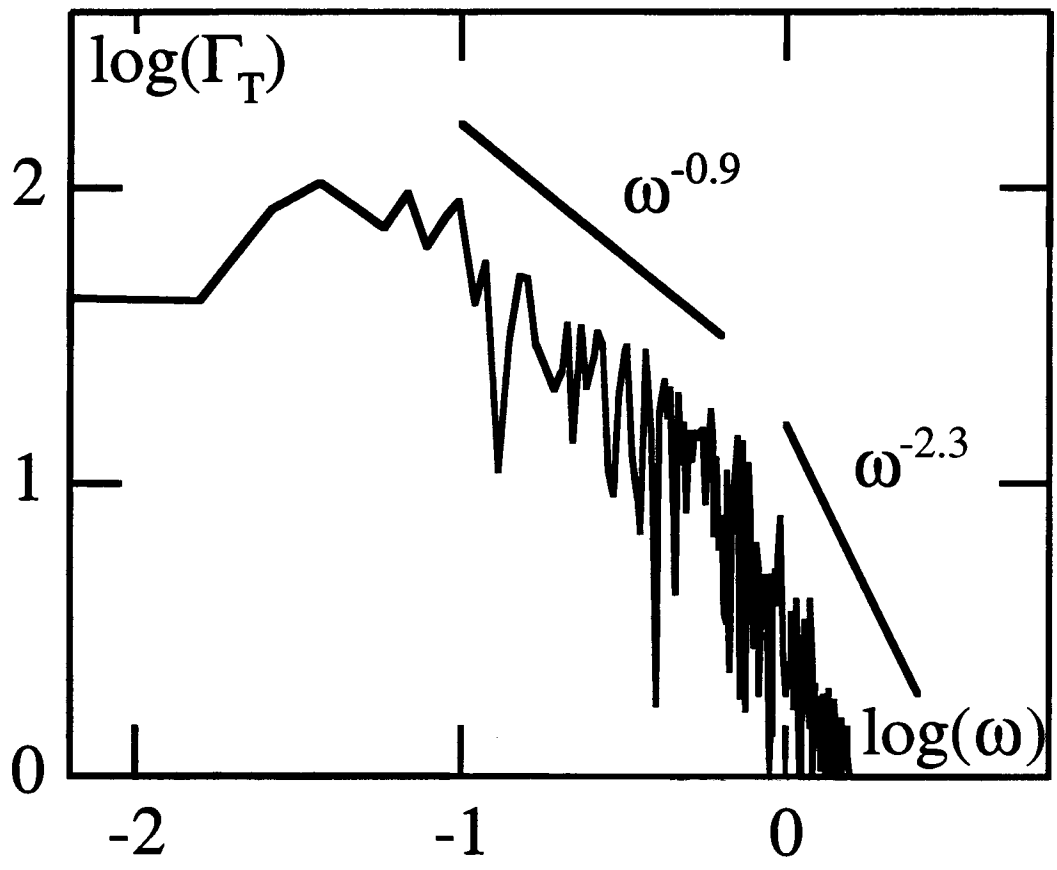

Fig.4

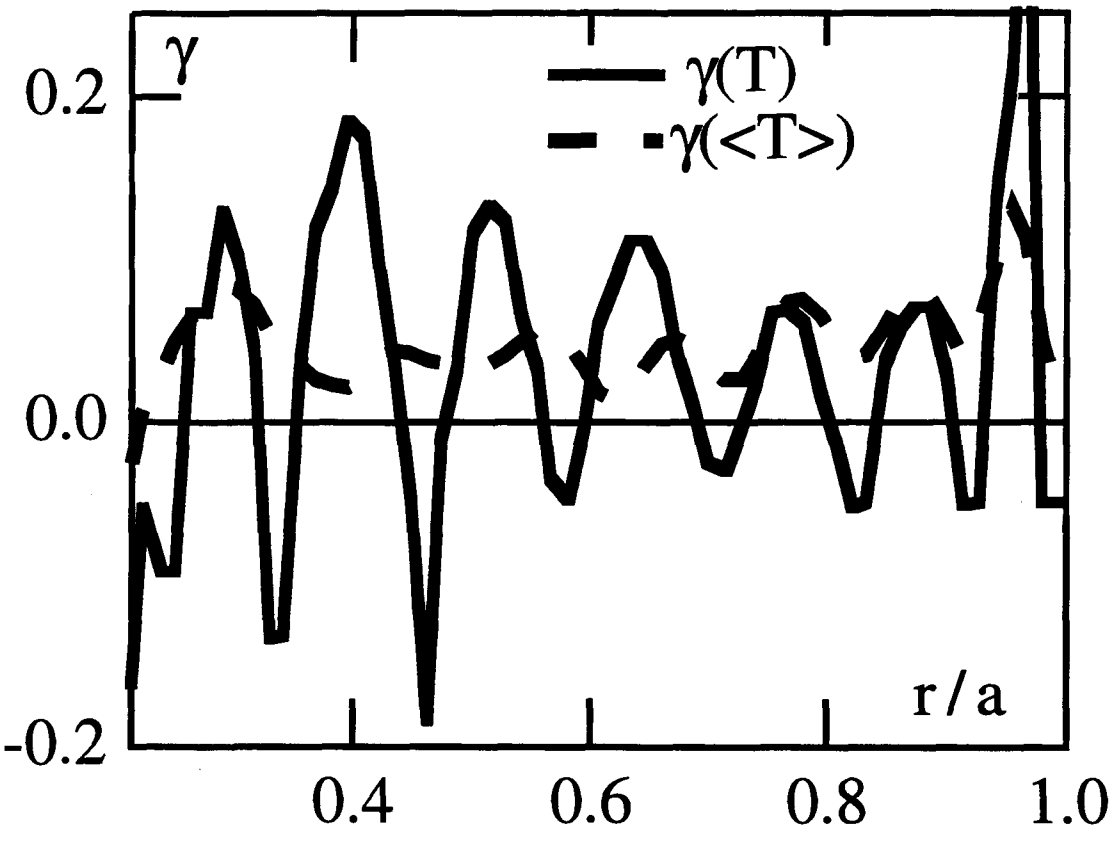

Fig.5

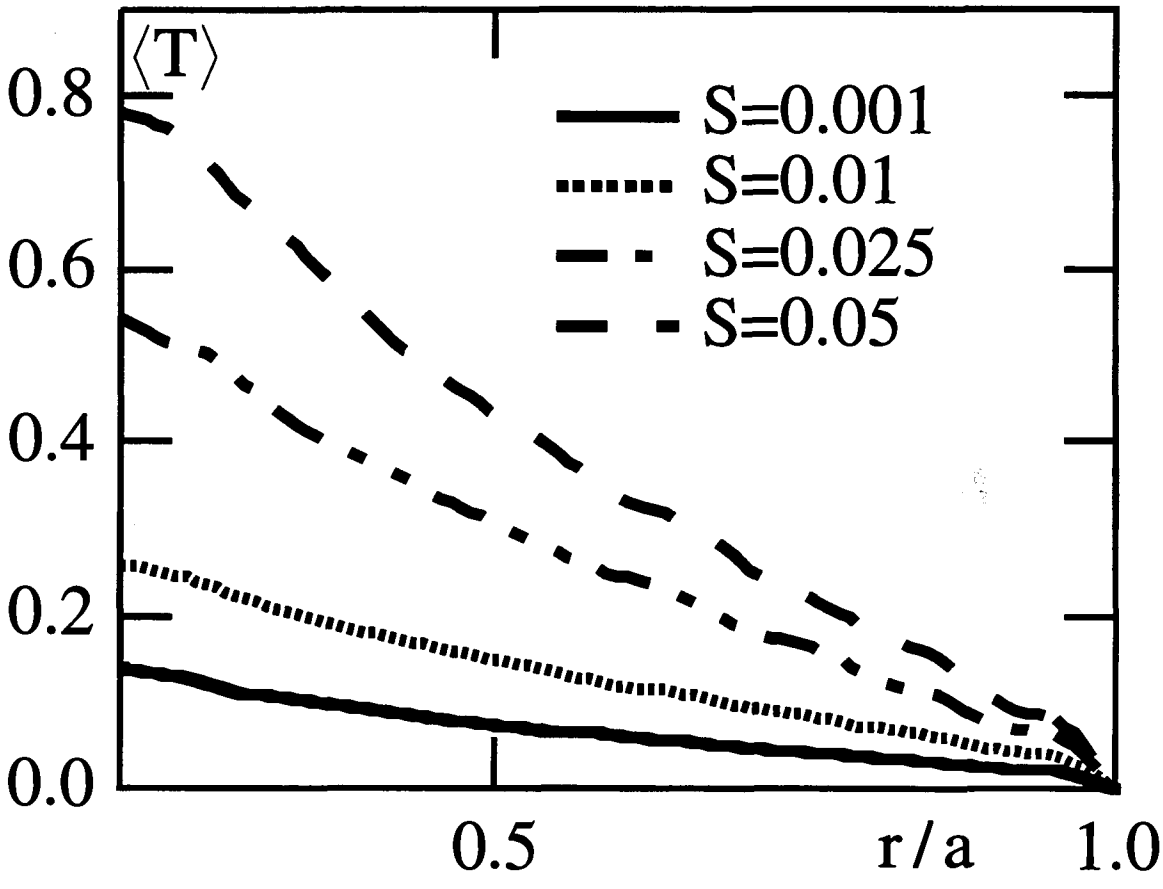

Fig.6

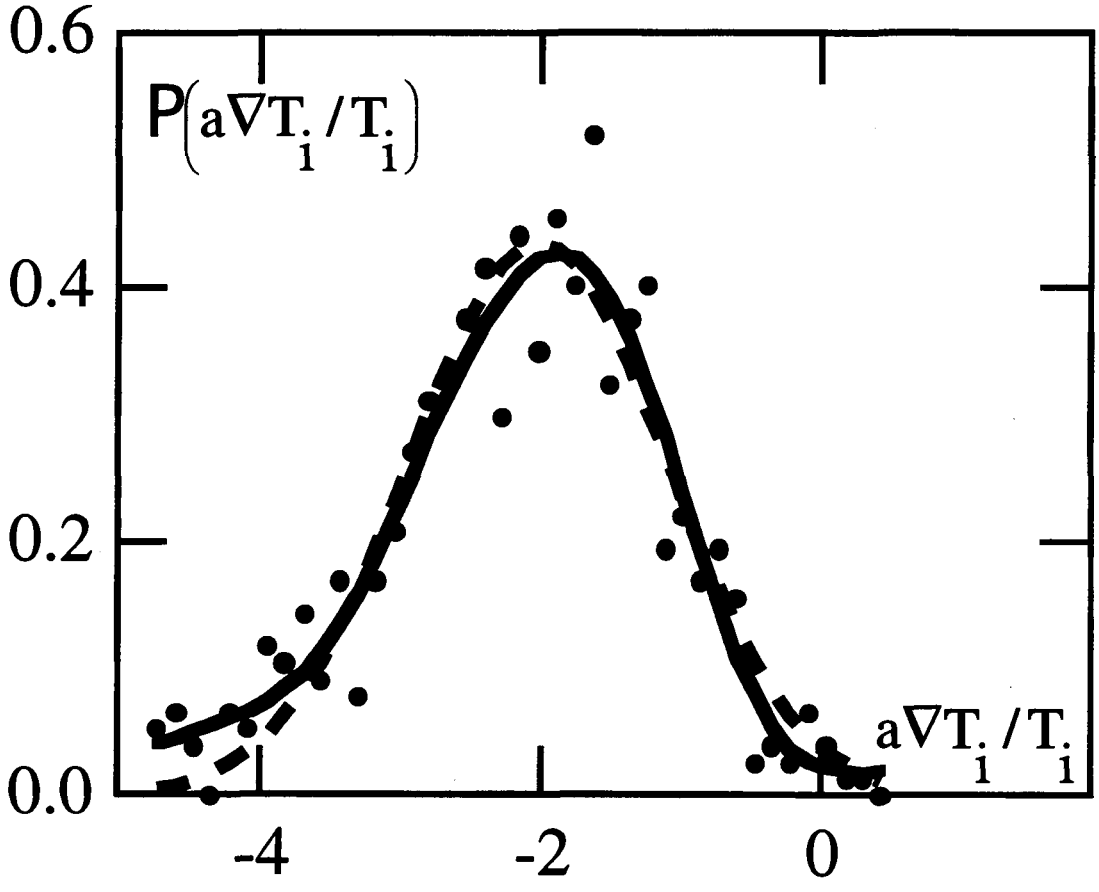

Fig.7

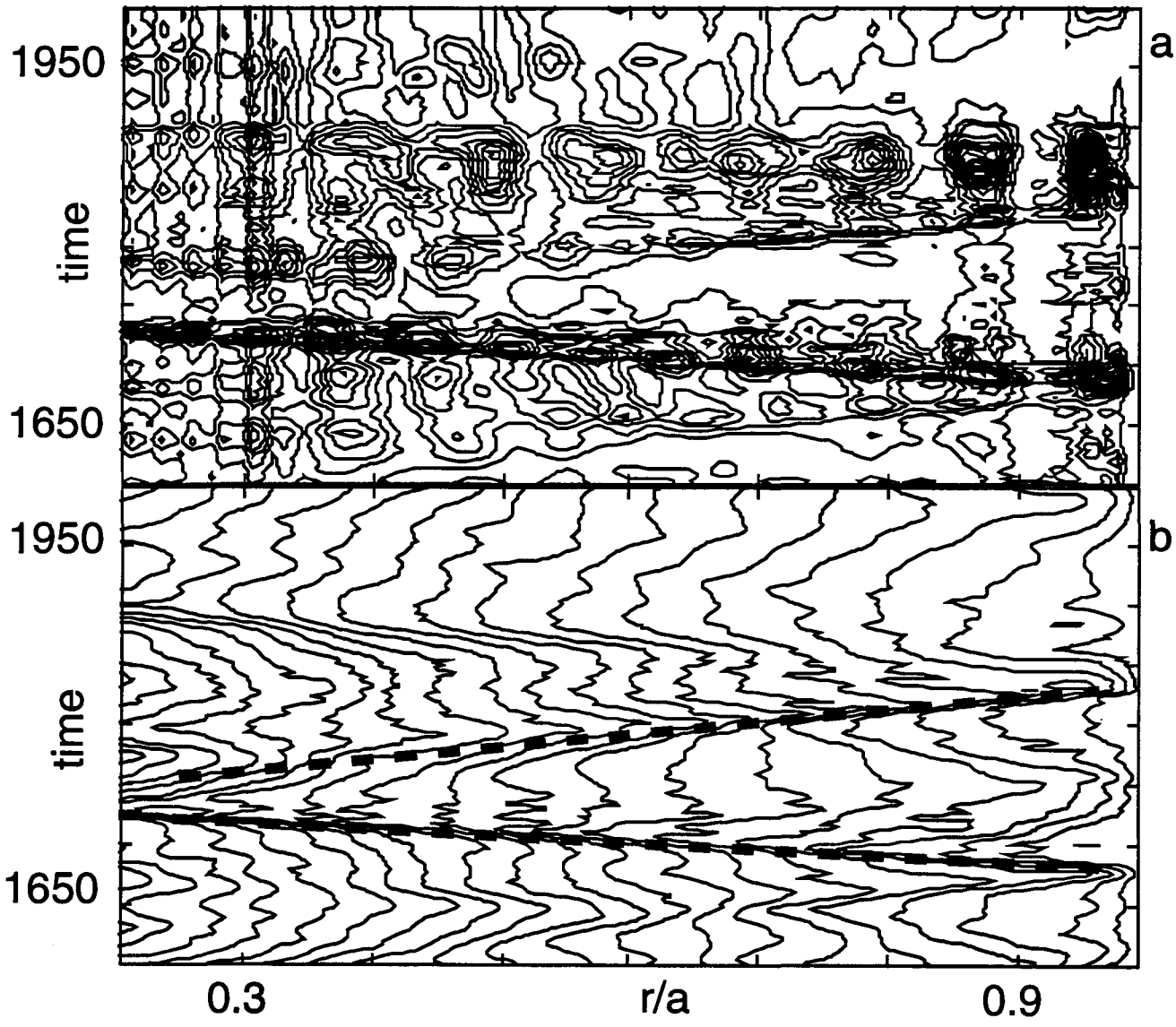

Fig.8

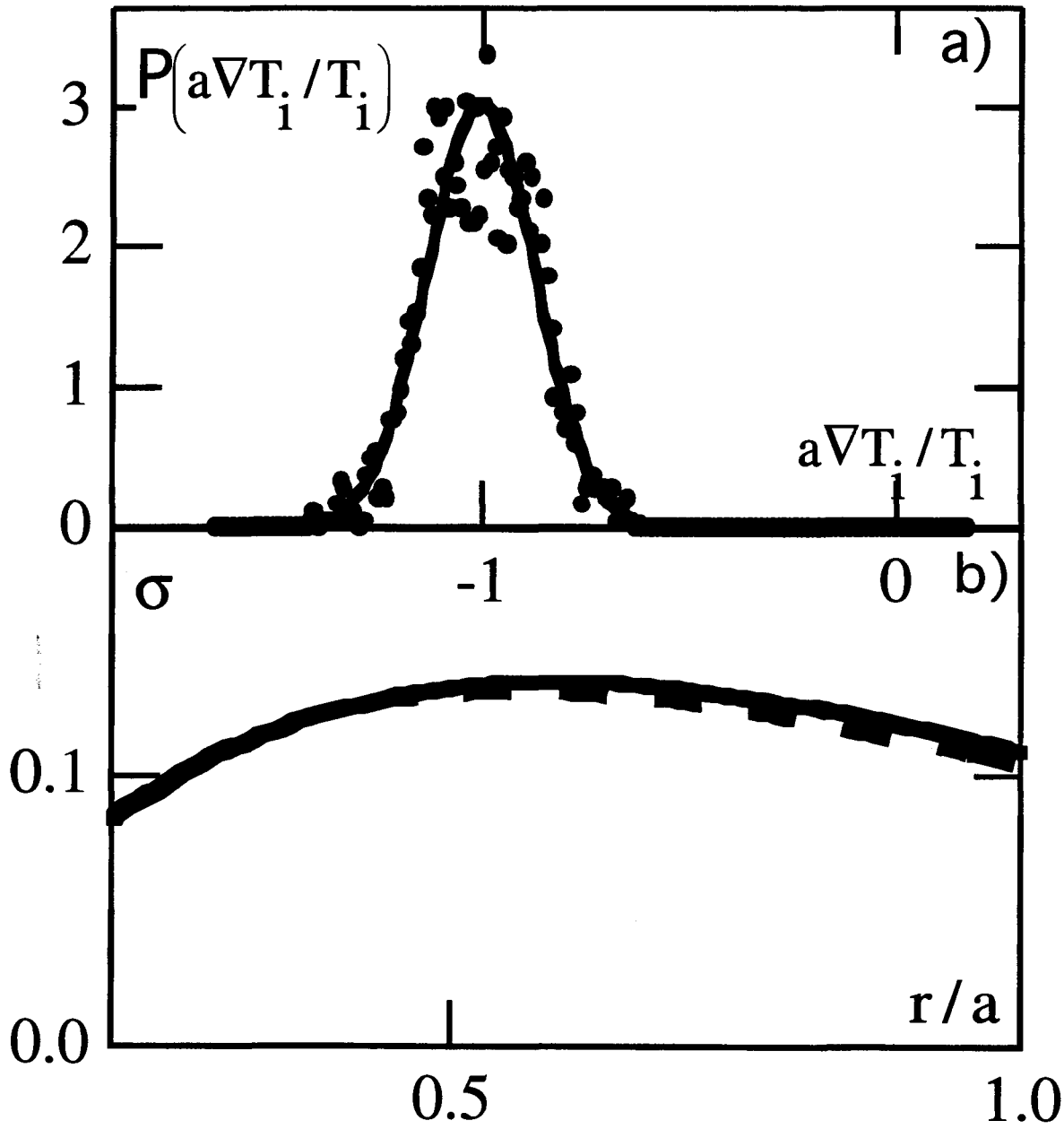

Fig.9

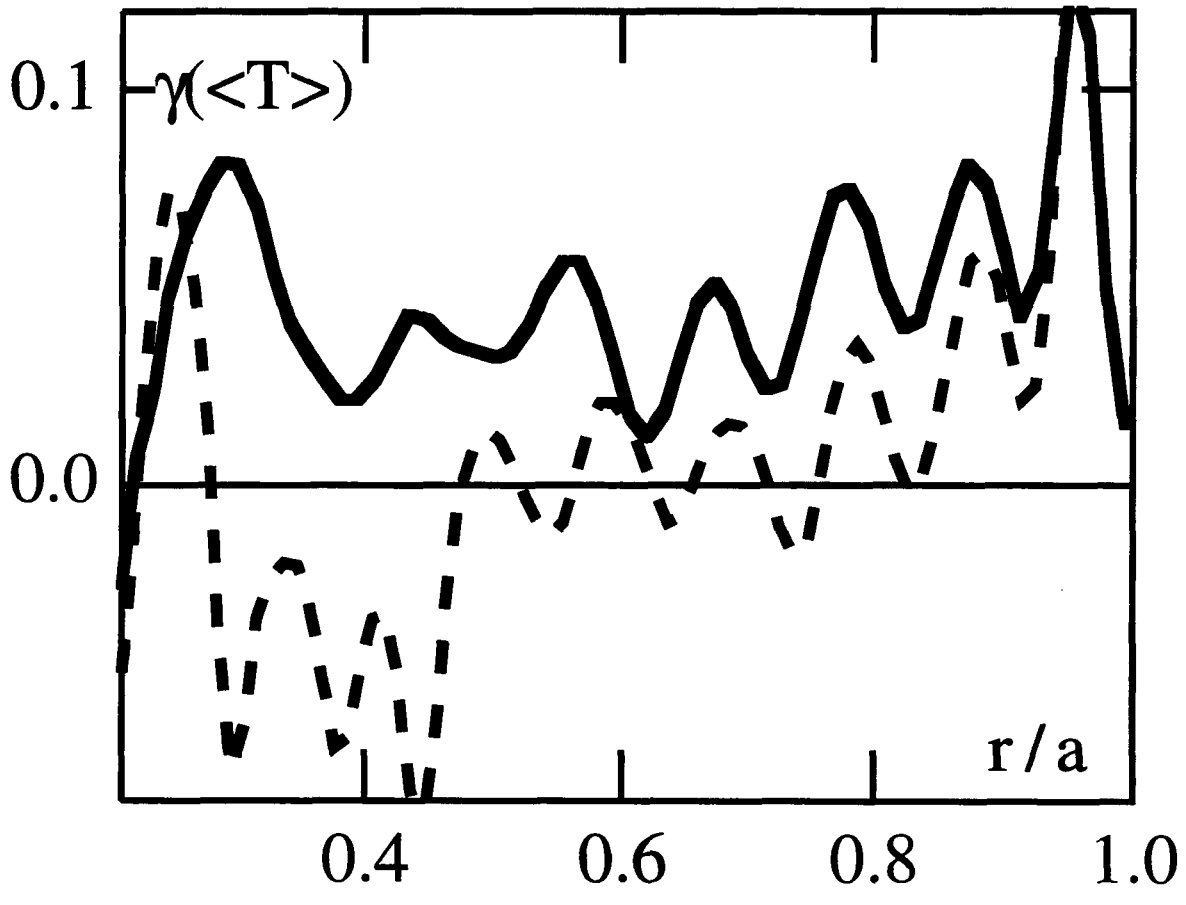

Fig.10

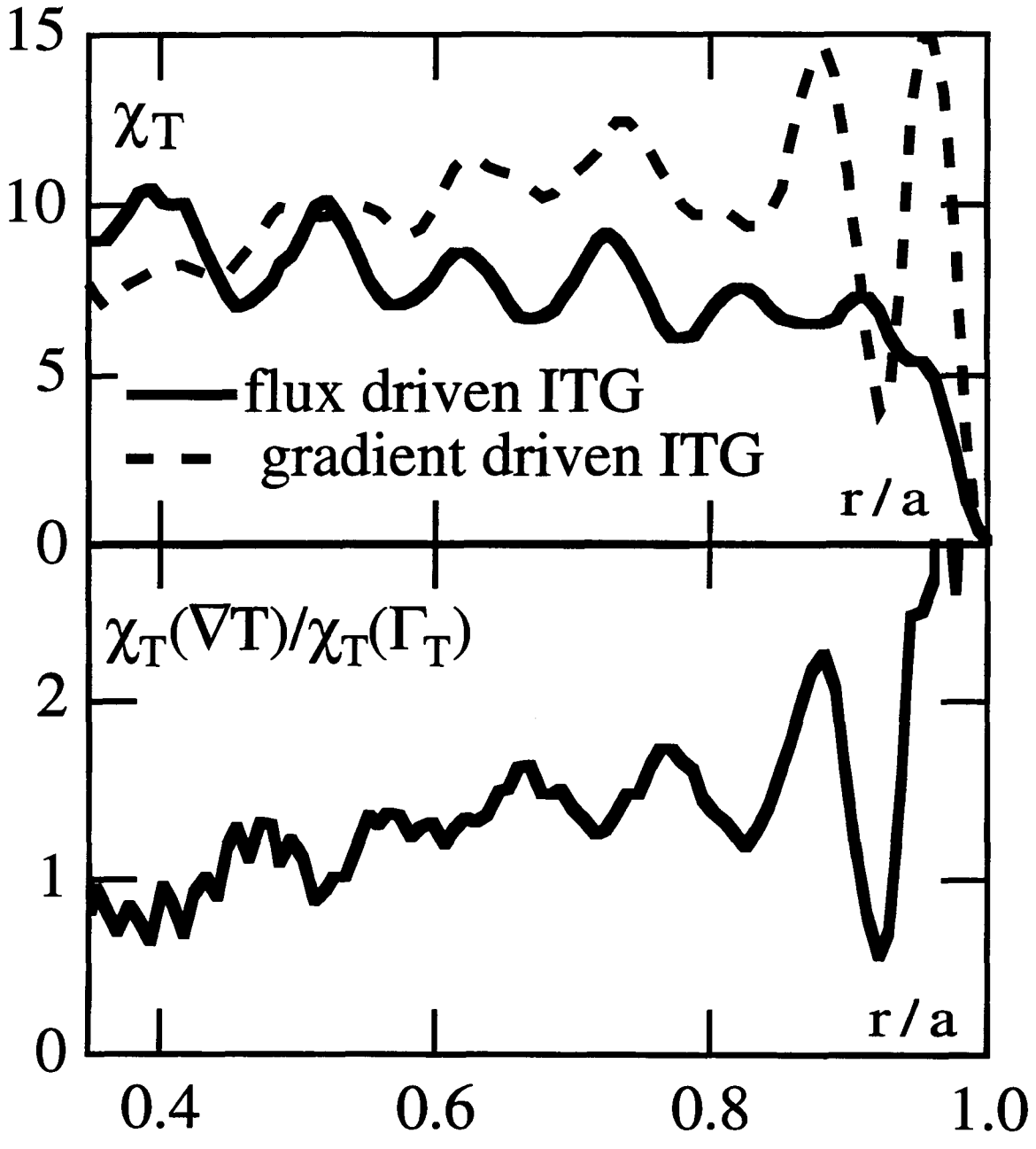
15
10
5
0
χ_T
flux driven ITG
gradient driven ITG
r/a
$\chi_T(\nabla T)/\chi_T(\Gamma_T)$
2
1
0
r/a
0.4
0.6
0.8
1.0

Fig.11